

Real Time Multi Organ Classification on Computed Tomography Images

Halid Ziya Yerebakan
 Siemens Medical Solutions
 Malvern, USA

halid.yerebakan@siemens-healthineers.com

Yoshihisa Shinagawa
 Siemens Medical Solutions
 Malvern, USA

yoshihisa.shinagawa@siemens-healthineers.com

Gerardo Hermosillo Valadez
 Siemens Medical Solutions
 Malvern, USA

gerardo.hermosillovaladez@siemens-healthineers.com

Abstract

Organ segmentation is a fundamental task in medical imaging, and it is useful for many clinical automation pipelines. Typically, the process involves segmenting the entire volume, which can be unnecessary when the points of interest are limited. In those cases, a classifier could be used instead of segmentation. However, there is an inherent trade-off between the context size and the speed of classifiers. To address this issue, we propose a new method that employs a data selection strategy with sparse sampling across a wide field of view without image resampling. This sparse sampling strategy makes it possible to classify voxels into multiple organs in real time without using accelerators. Although our method is an independent classifier, it can generate full segmentation by querying grid locations at any resolution. We have compared our method with existing segmentation techniques, demonstrating its potential for superior runtime in practical applications in medical imaging.

1. Introduction

Medical image segmentation has been a long-standing research topic within the healthcare and medical imaging communities, aimed at enhancing radiology workflows through automation. Compared to landmarking and bounding box detection methods, segmentation provides more granular information. This is beneficial for storing the anatomical locations of findings in structured databases, quantifying abnormalities, planning radiotherapy, calculating doses, comparing longitudinal studies, visualizing imaging data, or filtering the scanning region for CAD algorithms. Therefore, it is desirable to have fast and accurate segmentation algorithms in our medical vision pipelines.

The field of medical image segmentation has significantly evolved, transitioning from traditional methodologies to advanced deep learning algorithms and thereby achieving improvements in both the quality and speed of segmentation processes. A notable development in this domain has been the introduction of U-net and its variants, which leverage feature pyramid structures to combine global and local information, enhancing robustness and achieving higher resolution masks [11]. This approach has not only proved beneficial for medical image segmentation but has also found applicability in a broad range of segmentation tasks across general computer vision.

Recent advancements have introduced transformer architectures to overcome the limitations of convolutional networks' receptive fields, thus enabling superior segmentation outcomes in medical images [8, 9]. These methods harness token-to-token interactions across the entire field of view within small patches to capture long-range information. However, the architecture change introduces quadratic complexity in relation to the field of view, posing challenges for computational efficiency.

Independent classifiers are not commonly used for medical image segmentation because they are considered inefficient due to the repetitive computations required by the sliding window technique. Moreover, the absence of dependency between classification estimations in neighboring locations creates more irregular masks. However, they offer the advantage of quickly obtaining the organ label without needing to scan the entire input image. In this study, we demonstrate a method to reduce the computational burden of classifier-based segmentation using a data selection strategy. This strategy involves sparse sampling of intensities with a wide field of view in a hierarchical grid, similar to the approach of Yerebakan et al [18]. This selection strategy allows a machine learning classifier to label only query

locations with a reduced amount of data while maintaining segmentation-level accuracy. Furthermore, applying the classifier to a regular grid on an image at any resolution provides full-volume segmentation. We also describe a refinement operation that improves the granularity of masks by increasing resolution at edges. With this architecture, we can avoid significant computation and storage costs, making many applications practical, such as storing all user annotated findings with corresponding organ labels or organ-specific processing of input images without the need for full segmentation. In our experiments, we used the public BTCV dataset for evaluation. Classifying a single point takes about 0.92 ms, whereas fine-level segmentation takes around 10 s without requiring additional GPU hardware.

1.1. Related Work

Identifying organs for points within medical images can be approached through various anatomical intelligence methods. For example, landmarking techniques offer quick estimates of anatomical regions but have limited precision for specific organ labeling at arbitrary positions [5]. Similarly, object detection methods provide bounding box definitions but encounter limitations in precise organ boundaries. Atlas-based segmentation can accurately label organs, involving image registration to a predefined atlas. Thus, this approach is not preferred due to its high computational demands and the necessity of maintaining atlas images alongside their segmentations, making it less practical for real-time applications. Even strategies focusing on semantic feature matching to match points to an atlas [2, 16, 18] fail to achieve processing times under 100ms, indicating a gap in achieving real-time performance.

Organ classification, while less extensively explored than segmentation techniques, finds significant application in the MedMNIST dataset [17]. Although MedMNIST serves as an effective educational benchmark, its utility in real-world scenarios is limited due to varying views of organ fields, necessitating object detection to standardize image sizes for direct application. For that, Object detection, followed by classification, forms a pipeline approach but requires additional complexity. Xu et al. [15] demonstrated that organ bounding box detection of organs could be achieved in just 0.25 seconds using acceleration hardware. However, bounding boxes provide only a rough estimation and cannot pinpoint specific organ locations based on user interactions, such as a mouse click position. In contrast, organ segmentation offers a more detailed view than simple landmark detectors or bounding boxes, providing the granularity necessary for precise organ identification. Consequently, our research primarily focuses on exploring the alternatives of segmentation methods and specifically addressing the need for precomputation, which is costly.

U-Net, introduced by Ronneberger et al. [6, 11], has

become a baseline for segmentation algorithms for a considerable time. This architecture is initially designed for medical image segmentation using CNN architectures. U-Net's strength lies in its utilization of multiple image resolutions to extract feature vectors, allowing coarse layers to focus on global representations while finer levels handle local details. Several studies have modified various aspects of U-Net to enhance segmentation performance[19]. In our method, we also employ a similar multi-resolution strategy with a large field of view. However, instead of resampling the image volume, we have directly defined a sampler function to select intensities from the raw data with offset locations. This sampling mechanism allows the creation of independent descriptors at voxel locations, allowing rapid point-wise classifications.

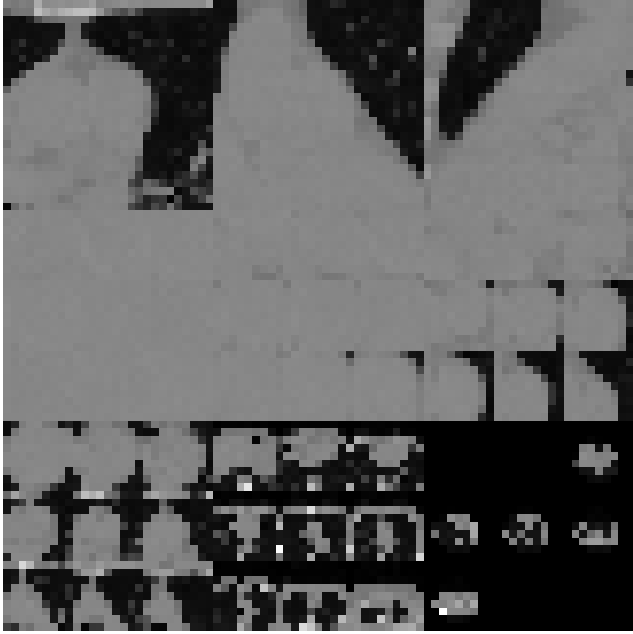
Recently, transformers have gained popularity in the medical imaging domain. UnetTr [9], in particular, has demonstrated superior performance compared to U-Net on the BTCV dataset. Subsequent improvements have addressed both computational efficiency and accuracy. For instance, SwinUnetTR [3] enhanced the UnetTr framework and shifted window strides in segmentation tasks. Despite these advancements, the computational time for these algorithms remains a challenge, especially for real-time applications, even when utilizing GPU hardware.

Foundational model approaches have gained popularity in medical vision, similar to Large Language Models in NLP. An example is Vox2Vec [7], which introduces an alternative method for learning directly from the image data without supervision. There are studies that also addressed pretraining self-supervised models for better segmentation accuracy [4]. These representation learning methods can create vectors for individual voxels that could be used for classification. Still, processing a large subvolume is necessary, even for a single point.

It is noteworthy that the dataset space for medical image segmentation tasks is also expanding. The Total Segmentation Dataset has published 1,204 images for 117 organs [14]. The model has been made available within the Monai¹ library and can be used directly as a command-line program. The algorithm's runtime is approximately 30 seconds on GPU and several minutes on CPU hardware. Additionally, there are various competitions in medical image segmentation. Among them, the Flare challenge aims for fast computation times, with the fastest methods clocking around 10 seconds using GPU hardware ²[10] in the 2022 leaderboard.



(a) Sampling Offsets For Descriptor Definition



(b) Decoding Image From A Descriptor

Figure 1. Descriptor Definition

2. Our Method

Our method consists of two steps. First, we perform multi-resolution sparse sampling around the point of interest and

then apply a deep neural network classifier to the collected descriptor. This process assigns an organ label to the selected point in the volumetric image.

2.1. Sparse Sampling Image Intensities

The resampling step is very common in medical image segmentation pipelines. It remains time-consuming for interactive use and requires additional memory. Instead of resampling the image, our method defines a sampler function with fixed millimeter offsets. Then, descriptors are just image intensities on those offset locations. This sampler works only on selected query points, significantly reducing the required computation for any point of interest in the image.

The organ label in a point of interest depends on the intensity values near the point itself. On the other hand, context plays a role in disambiguating similar-looking soft tissue types. Therefore, instead of sampling with a single resolution and a limited subvolume, we have used different regular grids at different resolutions for sampling to capture a large area in a hierarchical manner. Thanks to the consistency of the human body, similar anatomical locations generate similar descriptors. The fixed offsets behave like distance sensors that encode location.

The sampler offsets are in millimeters, and they are adjusted to voxel offsets once the image is loaded, using division by voxel spacing and rounding. Also, if the offset locations are outside the image volume, they are assigned a value of 0 for the corresponding dimension, ensuring all descriptors are in the same vector space. During runtime, descriptor computation involves only memory lookup operations. Memory positions come from adding offsets to the current query point. In our experiments, we have utilized 2D+3D grids for sampling. The 2D part consists of 3 orthogonal planes defined at a 4mm resolution by a 27x27 grid. The 3D part comprises six three-dimensional grids at resolutions of 2, 3, 5, 12, 28, and 64 mm, respectively, with 9x9x9 grid sizes considering some slice thickness in CT images. Spacing increased with non integer multipliers to avoid sampling the same locations in different resolution grids. Selection of size 9 grid allows both 2d and 3d to be present in the same picture simplifying debugging. We named this approach 3.5D sampling since it contains more than 3D information. Exemplary sampling grids in a single slice given a point are shown in Figure 1a, where bright dots are the sampling locations. The hierarchical nature of the sampling allows for a very large field of view with granular detail in the center. These descriptors can be decoded back into an 81x81 2D image as seen in Figure 1b by placing every 27x27 block in 9 different places. In this figure, the upper left corner is reserved for the 2D portion of the descriptor with three orthogonal planes, and the other parts are 3D slices at different resolutions with 9x9x9 grids. The total dimension of the descriptor becomes 6561. As seen in the

¹<https://monai.io/>

²<https://flare22.grand-challenge.org/testing-results/>

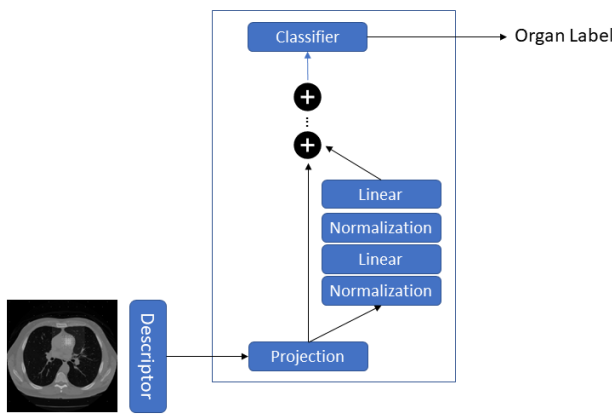


Figure 2. 1D Residual Network on Sampled Intensities

figure, the query location belongs to the heart. While other descriptor definitions are possible, for the sake of simple decoding for visualization, we used this $9 \times 9 \times 9 \times 9$ descriptor definition described here. The organ label is defined as the segmentation label at the query point.

2.2. Classification

We have chosen a 1D residual feedforward network as the classifier in this work. It is faster since there is only one multiplication per sampled point, and it does not have translation invariance since translations in the descriptor change the organ labels in the center of sampling. The classifier outputs the organ label probabilities given the sparsely sampled flat 1D descriptor at that point. Residual connections are implemented by two-layer linear blocks interleaved with normalization. After the initial projection, we used the same number of hidden dimensions until the last classifier layer. Since the full descriptor is passed as a 1D input, all resolutions are fused in the middle layers. The model architecture is visualized in Figure 2. Swish activation functions are used after the linear layers. Projection is the most computational part of the classifier due to $6561 \times n_{\text{hidden}}$ number of parameters where n_{hidden} is smaller than the initial descriptor size.

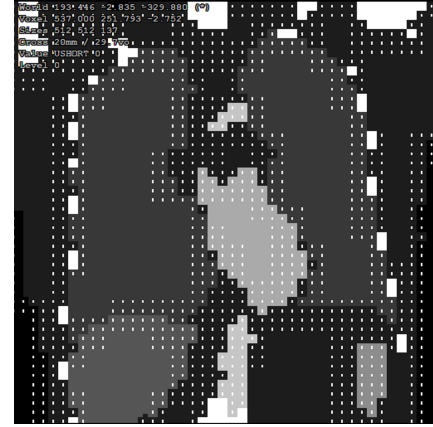
2.3. Segmentation

The classifier provides a functionality to get an organ label for any query location. Thus, it is possible to compute a segmentation mask by independently querying all voxels. However, querying every location in the image is computationally expensive. Instead, we can use a sparse grid with any resolution to obtain faster results.

The high-level 8mm sparse grid would create a coarse segmentation mask, as shown in an example in Figure



(a) Coarse Segmentation



(b) Edge Refinement



(c) Fine Details

Figure 3. Classifier based segmentation allows to create segmentation masks in different resolutions without need of any change

3a where each intensity represents a different organ label. Once this mask is generated, the whole volume could be filled with nearby labels. However, masks are not accurate near edges due to low resolution.

Since errors are happening on the edges, we could further refine the resolution in those regions in a hierarchical

way. To achieve this, we have checked all points in the segmentation mask with higher resolution and added points into the task queue for the query if the neighbors have different labels, as shown in Figure 3b. For each level, we have some smoothing on the edges by thresholding a majority of 20 within 27 neighbors to prevent excessive computation. Thus, the cost of classification in high resolution at nearly homogeneous points would be eliminated. We reduced spacing to 2mm with this approach. An example generated mask is shown in Figure 3c. Thanks to points being completely independent of each other, there is a massive parallelization potential.

3. Experiments

We have experimented with our method on the public BTCV dataset. It contains a total of 30 images with 13 abdominal organ labels. We trained with 24 cases and used the validation part of the official split, which consists of 6 images for evaluation similar to compare studies. The data is accessible online ³.

For the training dataset generation, we have sampled random locations globally and random locations from each class. The latter provides some balancing to labels, which could be adjusted. In our experiments, we have used 100k examples per training image, of which 10% belong to the balanced set. The corresponding classifier label is obtained from the center voxel of the mask image. The image descriptors are divided by 128 and clipped between -4 and 4.

We have used 8 layers of neural network with 128 dimensions mostly considering performance constraints. Our initial learning rate is 3e-4, with cosine decay reducing the learning rate down to 1e-6. L1-L2 regularization is used with 1e-5 coefficient in addition to 0.25 drop out ratio. The model is trained for 100 epochs on standard cross-entropy loss. We did not add any data augmentation. In fact, random flips are against the positional priors of the human body if images are loaded correctly, especially in the abdomen region, but small random rotations could be helpful.

Once the model is trained, it is converted to C++ counterpart to reduce latency. We have used OpenMP parallelization for different query points for segmentation part of the experiment. Time has measured on 6 core - 12 thread CPU.

In the classification part, we had 1000 calls to validation set in random locations and compared against ground truth. Total time is measured for each case, and average time is calculated. The average time per query is 0.92 ± 0.01 milliseconds. With this speed, we are able to obtain 97.4% accuracy with a macro average 86.76% F1 score, including background class in the classification task. The classifier speed is similar across different volumes since volume size does not have a direct impact on descriptor size.

³<https://www.synapse.org/#!Synapse:syn3193805/wiki/217789>

In the segmentation part, we first obtained coarse segmentation for full volume. An example 2d slice is shown in Figure 4b. The average coarse segmentation speed is 5.24 ± 0.9 s per volume. Segmentation is also refined in the edges using the same classifier. The speed, in this case, is an average of 9.51 ± 2.72 s on the CPU. We measured dice scores and compared them against recently published studies on the same set. In terms of runtime speed, Shaker et. al. [12] reports GPU time of 62.4 seconds while being the most efficient algorithm therein. The results are shown in Table 1.

Our algorithm, on average, reaches a dice score of 65.96 without any augmentation or additional training data. Despite being lower as compared to full volume segmentation this value defines a new benchmark for a new category of point classification based segmentation methods.

4. Discussion

It is possible to improve the proposed system in various ways. We list some of them in this section.

A connected component analysis could be further included to remove false positive errors in the segmentation masks before refinement. The biggest connected component could be selected to remove erroneous regions before further refining the edges. This method is likely to improve both the speed and the accuracy of the system.

The independence of the classifier is a limitation in segmentation operation. It is possible to create an additional filter on extracted class probabilities further to reduce the variance within local estimations. Another alternative is utilizing independent classifier features as token embedding for further transformer layers instead of processing full 3D raw data. However, in this case, real-time response needs to be sacrificed. The power of an independent classifier is that it works on any resolution and any interest region without the need for full-volume processing.

5. Conclusion

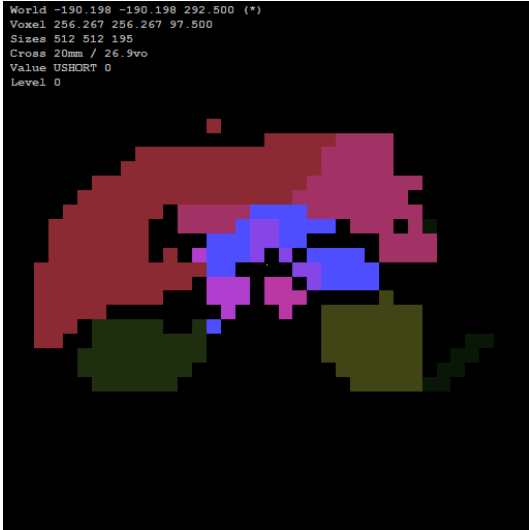
We have demonstrated an efficient multi-organ classification algorithm that can produce organ labels in real time. This algorithm could be utilized further to create segmentation masks for full 3d CT volumes within seconds without additional hardware. Despite the loss in accuracy, the runtime advantage makes it amenable to many practical use cases. The proposed data selection strategy's advantages extend beyond enhancing segmentation efficiency; it holds the potential to accelerate a variety of medical imaging tasks, including object detection, registration, and landmarking. In the future, we are considering experimenting with more organs and alternative deep learning architectures.



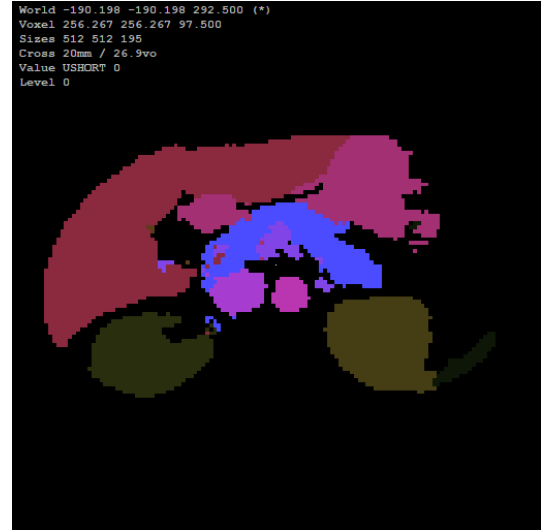
(a) Image Slice



(b) Ground Truth Mask



(c) Coarse Segmentation



(d) Fine Mask

Figure 4. Qualitative Results on BTCV dataset

Table 1. Dice Score Averages on Multi Organ Segmentation on BTCV validation set

Methods	Spleen	RKid	LKid	Gall	Eso	Liv	Sto	Aor	IVC	Veins	Pan	RAG	LAG	AVG
From Scratch														
ViT3D-B [4]	0.8902	0.8926	0.8769	0.4763	0.4891	0.9447	0.7475	0.8207	0.773	0.6175	0.6442	0.5663	0.4699	0.7084
nnFormer [12]	0.9458	0.8862	0.9368	0.6529	0.7622	0.9617	0.8359	0.8909	0.8080	0.7597	0.7787	0.7020	0.6605	0.8162
UnetTR++ [12]	0.9494	0.9190	0.9362	0.7075	0.7718	0.9595	0.8515	0.8928	0.8314	0.7691	0.7742	0.7256	0.6817	0.8328
Pretrained														
ViT3D-L[4]	0.9556	0.9582	0.9414	0.5206	0.5352	0.9898	0.8025	0.8811	0.8298	0.6649	0.6916	0.6088	0.5045	0.7603
Ours	0.8398	0.8364	0.7990	0.4780	0.6489	0.9264	0.6860	0.7770	0.7106	0.5007	0.5583	0.4054	0.4089	0.6596

References

- [1] Reza Azad, Leon Niggemeier, Michael Hüttemann, Amirhossein Kazerouni, Ehsan Khodapanah Aghdam, Yury

Velichko, Ulas Bagci, and Dorit Merhof. Beyond self-attention: Deformable large kernel attention for medical image segmentation. In *Proceedings of the IEEE/CVF Winter*

- ter Conference on Applications of Computer Vision, pages 1287–1297, 2024.
- [2] Xiaoyu Bai and Yong Xia. Sam++: Enhancing anatomic matching using semantic information and structural inference. *arXiv preprint arXiv:2306.13988*, 2023. 2
- [3] Hu Cao, Yueyue Wang, Joy Chen, Dongsheng Jiang, Xiaopeng Zhang, Qi Tian, and Manning Wang. Swin-unet: Unet-like pure transformer for medical image segmentation. In *European conference on computer vision*, pages 205–218. Springer, 2022. 2
- [4] Zekai Chen, Devansh Agarwal, Kshitij Aggarwal, Wiem Safta, Mariann Micsinai Balan, and Kevin Brown. Masked image modeling advances 3d medical image analysis. In *Proceedings of the IEEE/CVF Winter Conference on Applications of Computer Vision*, pages 1970–1980, 2023. 2, 6
- [5] Florin C Ghesu, Bogdan Georgescu, Sasa Grbic, Andreas K Maier, Joachim Hornegger, and Dorin Comaniciu. Robust multi-scale anatomical landmark detection in incomplete 3d ct data. In *International Conference on Medical Image Computing and Computer-Assisted Intervention*, pages 194–202. Springer, 2017. 2
- [6] Eli Gibson, Francesco Giganti, Yipeng Hu, Ester Bonmati, Steve Bandula, Kurinchi Gurusamy, Brian Davidson, Stephen P Pereira, Matthew J Clarkson, and Dean C Barratt. Automatic multi-organ segmentation on abdominal ct with dense v-networks. *IEEE transactions on medical imaging*, 37(8):1822–1834, 2018. 2
- [7] Mikhail Goncharov, Vera Soboleva, Anvar Kurmukov, Maxim Pisov, and Mikhail Belyaev. vox2vec: A framework for self-supervised contrastive learning of voxel-level representations in medical images. In *International Conference on Medical Image Computing and Computer-Assisted Intervention*, pages 605–614. Springer, 2023. 2
- [8] Ali Hatamizadeh, Vishwesh Nath, Yucheng Tang, Dong Yang, Holger R Roth, and Daguang Xu. Swin unetr: Swin transformers for semantic segmentation of brain tumors in mri images. In *International MICCAI Brainlesion Workshop*, pages 272–284. Springer, 2021. 1
- [9] Ali Hatamizadeh, Yucheng Tang, Vishwesh Nath, Dong Yang, Andriy Myronenko, Bennett Landman, Holger R Roth, and Daguang Xu. Unetr: Transformers for 3d medical image segmentation. In *Proceedings of the IEEE/CVF winter conference on applications of computer vision*, pages 574–584, 2022. 1, 2
- [10] Andriy Myronenko, Dong Yang, Yufan He, and Daguang Xu. Automated segmentation of organs and tumors from partially labeled 3d ct in miccai flare 2023 challenge. 2023. 2
- [11] Olaf Ronneberger, Philipp Fischer, and Thomas Brox. Unet: Convolutional networks for biomedical image segmentation. In *Medical Image Computing and Computer-Assisted Intervention—MICCAI 2015: 18th International Conference, Munich, Germany, October 5–9, 2015, Proceedings, Part III 18*, pages 234–241. Springer, 2015. 1, 2
- [12] Abdelrahman Shaker, Muhammad Maaz, Hanoona Rasheed, Salman Khan, Ming-Hsuan Yang, and Fahad Shahbaz Khan. Unetr++: delving into efficient and accurate 3d medical image segmentation. *arXiv preprint arXiv:2212.04497*, 2022. 5, 6
- [13] Ryu Tadokoro, Ryosuke Yamada, and Hirokatsu Kataoka. Pre-training auto-generated volumetric shapes for 3d medical image segmentation. In *Proceedings of the IEEE/CVF Conference on Computer Vision and Pattern Recognition*, pages 4739–4744, 2023.
- [14] Jakob Wasserthal, Hanns-Christian Breit, Manfred T Meyer, Maurice Pradella, Daniel Hinck, Alexander W Sauter, Tobias Heye, Daniel T Boll, Joshy Cyriac, Shan Yang, et al. Totssegmentator: Robust segmentation of 104 anatomic structures in ct images. *Radiology: Artificial Intelligence*, 5(5), 2023. 2
- [15] Xuanang Xu, Fugen Zhou, Bo Liu, Dongshan Fu, and Xiangzhi Bai. Efficient multiple organ localization in ct image using 3d region proposal network. *IEEE transactions on medical imaging*, 38(8):1885–1898, 2019. 2
- [16] Ke Yan, Jinzheng Cai, Dakai Jin, Shun Miao, Dazhou Guo, Adam P Harrison, Youbao Tang, Jing Xiao, Jingjing Lu, and Le Lu. Sam: Self-supervised learning of pixel-wise anatomical embeddings in radiological images. *IEEE Transactions on Medical Imaging*, 41(10):2658–2669, 2022. 2
- [17] Jiancheng Yang, Rui Shi, Donglai Wei, Zequan Liu, Lin Zhao, Bilian Ke, Hanspeter Pfister, and Bingbing Ni. Medmnist v2-a large-scale lightweight benchmark for 2d and 3d biomedical image classification. *Scientific Data*, 10(1):41, 2023. 2
- [18] Halid Ziya Yerebakan, Yoshihisa Shinagawa, Mahesh Ranjanath, Simon Allen-Raffi, and Gerardo Hermosillo Valadez. A hierarchical descriptor framework for on-the-fly anatomical location matching between longitudinal studies. *CoRR*, abs/2308.07337, 2023. 1, 2
- [19] Zongwei Zhou, Md Mahfuzur Rahman Siddiquee, Nima Tajbakhsh, and Jianming Liang. Unet++: A nested u-net architecture for medical image segmentation. In *Deep Learning in Medical Image Analysis and Multimodal Learning for Clinical Decision Support: 4th International Workshop, DLMIA 2018, and 8th International Workshop, ML-CDS 2018, Held in Conjunction with MICCAI 2018, Granada, Spain, September 20, 2018, Proceedings 4*, pages 3–11. Springer, 2018. 2